CHAPTER

Serial block-face scanning electron microscopy of *Schmidtea mediterranea*

9

Melainia L. McClain[a] and Stephanie H. Nowotarski[a,b,*]

[a]*Stowers Institute for Medical Research, Kansas City, MO, United States*
[b]*Howard Hughes Medical Institute, Chevy Chase, MD, United States*
**Corresponding author. e-mail address: stn@stowers.org*

Chapter outline

Abstract

The flatworm planarian, *Schmidtea mediterranea* (*Smed*) is a master at regenerating and rebuilding whole animals from fragments. A full understanding of *Smed's* regenerative capabilities requires a high-resolution characterization of organs, tissues, and the adult stem

Methods in Cell Biology, Volume 177, ISSN 0091-679X, https://doi.org/10.1016/bs.mcb.2023.01.013

cells necessary for regeneration in their native environment. Here, we describe a serial block face scanning electron microscopy (SBF-SEM) protocol, optimized for *Smed* specifically, for visualizing the ultrastructure of membranes and condensed chromosomes in this model organism.

1 Introduction

Many animals can perform some form of regeneration as part of their ability to maintain tissues, but relatively few organisms that we know of can do so on a large scale after injury as adults. Arguably, one of the best at tissue regeneration are planarian flatworms. Planarian flatworms are bilaterian, free-living invertebrates from the Platyhelminthes phylum found in both freshwater and marine environments. From elegant historical experiments, we know they can be cut into minute pieces and still regenerate a whole animal from a fragment only 279th of the animal's original size (Morgan, 1898), a volume on the order of ~10,000 cells (Coward, 1968; Montgomery & Coward, 1974).

While at first glance the planarian body plan might seem simple compared to humans (Fig. 1), they contain, and can regenerate, relatively complex tissue and organs analogous to ours, arising from all 3 germ layers. All of these organs and cell types arise from adult pluripotent stem cells called neoblasts (Reddien & Sánchez Alvarado, 2004). Neoblasts are the only dividing cells in the animal (Baguñà, 1976; Newmark & Sánchez Alvarado, 2000; Orii, Sakurai, & Watanabe, 2005; Salvetti, Rossi, Deri, & Batistoni, 2000), are required for regeneration (Baguñà, Saló, & Auladell, 1989) and are contained throughout the body; neoblasts are absent only from the area anterior to the photoreceptors and the digestive organ (Newmark & Sánchez Alvarado, 2000). Current research seeks to understand the cellular-level specification and regulation of these plentiful adult stem cells, which requires a thorough characterization and understanding of their morphology and their local environment.

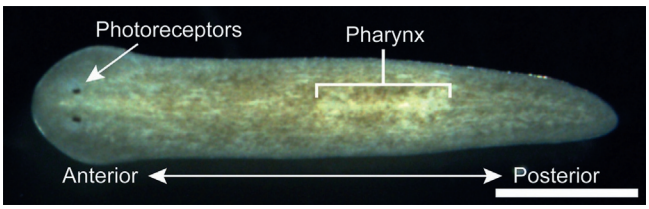

FIG. 1

Gross Anatomy of Smed. Bright field image of *Schmidtea mediterranea*. Scale bar is 1 mm.

Historically, neoblast morphology has been addressed by beautiful transmission electron microscopy (TEM) work (Hori, 1992; Morita, 1967; Morita, Best, & Noel, 1969; Pedersen, 1959). From this work and others, we know that neoblasts are present in the parenchyma, contain little cytoplasm, have few organelles and possess a special non-membrane bound organelle called the "chromatoid body" (Auladell, Garcia-Valero, & Baguñà, 1993; Hay & Coward, 1975; Hori, 1982; Morita et al., 1969). The chromatoid body is an RNP complex involved in PIWI-mediated RNA (piRNA) silencing of histones and transposable elements (Kim et al., 2019; Rouhana, Weiss, King, & Newmark, 2014; Solana, Lasko, & Romero, 2009). The limits of two-dimensional electron microscopy (2D EM) do not allow for understanding the volumetric fine structure of organelles, especially the chromatoid bodies and total cell morphology (e.g., cell projections and organelle distribution).

To better understand morphology of tissue volumes at high resolution, we must turn to three-dimensional electron microscopy (3D EM) techniques. While high-resolution options for light microscopy are becoming increasingly available, challenges such as high lipid content, presence of pigmentation and current lack of genetic tagging limit this method's utility. Combined with the inherent restriction of context via markers in light microscopy, these challenges present hurdles to understanding flatworm biology from the organellar level all the way to tissues and organs. Instead, 3D EM must take up this mantle and is poised to do so via multiple methods, each with its own advantages, limitations, and considerations (Table 1).

3D EM started with serial sections in TEM. This technique is limited by the area available on the required TEM imaging substrate and by the high skill level and excessive amount of time necessary to prepare and image large numbers of sections. Despite these limitations, this technique was still used to great effect, for example, in the first connectome *in C. elegans* (White, Southgate, Thomson, & Brenner, 1986). Advances in technology and software, as well as increased computer capacity in general, opened up possibilities for acquiring larger 3D EM datasets (Peddie et al., 2022). Array tomography techniques developed for SEM reduced spatial constraints by increasing substrate options for placing sections, such as coverslips, slides, tape and silicon wafers. Array tomography allows both larger and more sections to be cut and placed together on one substrate, enabling both larger fields of view and larger volumes. An example of using this technique is the *Macrostomum lignano* atlas (Grudniewska et al., 2018). However, sections cut and placed on any substrate as they are for the above techniques will suffer from some amount of unavoidable compression and distortion between each section due to the cutting process, which can make registration of the images a challenge.

SBF-SEM bypasses the problems associated with imaging sections by imaging the block-face instead. In this automated technique, a microtome similar to those used in cutting sections on a substrate is mounted inside the sample chamber of an SEM and used to cut away sections of a chosen thickness, imaging between each

Table 1 3D EM preparation strategies comparison.

Method	Pixel resolution/ detail clarity	Z Resolution (typical)	Volume	Field of view	Relative difficulty	Image alignment	Archival v. Destructive	Use When:
Manual serial sections on grids	Highest	50–100 nm	Small	Small	High	More difficult	Archival	If your area of interest is smaller than 1 mm and you need high X, Y resolution
Manual serial sections on substrate	Medium	50–100 nm	Medium	Medium-Large	High	More difficult	Archival	If you need only a few hundred sections or a larger area <3 mm
Automated serial sections on substrate	Medium	50–100 nm	High	Medium-Large	High	More difficult	Archival	If you need many hundreds to thousands of sections, higher X and Y resolution, and the flexibility to go back and re-image sections
FIB-SEM	Medium	4–10 nm	High	Small	Medium	Less difficult	Destructive	If your area of interest is small, you don't need the highest X and Y resolution, you want an isotropic data set at a higher resolution, you don't need to re-image sections
SBF-SEM	Lowest	30–100 nm	Medium	Small	Medium	Less difficult	Destructive	If your area of interest is <1 mm, you don't need the highest resolution/clarity, and you won't need to re-image sections

slice to build up a volume. This eliminates the problems of collecting and imaging sections and enables cutting and imaging of relatively large volumes with relatively little difficulty. As with all imaging approaches, SBF-SEM comes with its own drawbacks, in the form of increased sample preparation difficulty and the limitation of its destructive nature.

In deciding which 3D EM technique to use for interrogating neoblasts and their surrounding environment, the inherent ability of planarians to proportionally scale down when starved (indeterminate growth) (Oviedo, Newmark, & Sánchez Alvarado, 2003) makes SBF-SEM a good choice (Pellettieri et al., 2010), as a very large portion and possibly a whole animal is within a suitable size range for both processing and imaging using this technique. In order to get the largest portion of the region of interest, we determined that an XY resolution of 15 nm and a Z resolution of 60 nm would be sufficient for balancing area of interest versus pixel resolution while taking time constraints into consideration. This is well within the achievable resolution of SBF-SEM, and combined with the advantage of automated data collection made SBF-SEM the clear choice for our needs. With these resolutions it is now possible to interrogate questions like the organellar composition of neoblasts, the cell and tissue level interactions of dividing cells, and the location and environment around cell death. At a tissue level, questions around cellular morphology and relationship to other tissues and organs over development are tractable. While most of the phylum can regenerate, one of the most frequently studied species in the laboratory at present is *Smed*. Here, we present a SBF-SEM protocol for *Smed*, with suggestions on how to likely adapt the protocol for other species.

2 Rationale

We decided to use SBF-SEM imaging in our work identifying dividing cells in *Smed* because it could provide us with the necessary resolution with sufficiently large volumes per sample in a reasonable time frame, and the array tomography benefits of having archival sections and slightly higher resolution were not necessary for this work. Given that previous reports in *Smed* and other closely related flatworms had reported neoblasts to be in the 5–10 μm size range (Reddien & Sánchez Alvarado, 2004), we prioritized maximizing volume size and speed over archival sections and higher resolution, in order to capture as many dividing cells as possible within a timeframe of <2 months per sample. The automation and easier post processing associated with SBF-SEM were key advantages for maximizing the number of dividing cells we could capture.

3 Methods

3.1 Materials and equipment

- Nitrile Gloves
- 1.5–2.0 μL microcentrifuge tubes

  - Some find glass easier to prevent sample sticking
- 3 mm plastic pipettes and 1.5 mL thin tipped plastic pipettes
  - Some find glass easier to prevent sample sticking
- 10 mL syringes *(and additional sizes if needed)*
- Sterile syringe filters *(0.2 μm pore size)*
- Embedding molds *(Ted Pella #105)*
- Beem capsules *(Electron Microscopy Sciences #70021)*
- Glass knives (*for ultramicrotome)*
- Sample mounting pins appropriate for your SBF-SEM system
  - Gatan 3View SEM pin stubs (Electron Microscopy Sciences #75959-02; 75959-04)
- Razor blades
- Petri Dish
- Wood Applicator Sticks (*Electron Microscopy Sciences #72300)*
- Glass Slides
- Ice or Ice pack *(optional)*
- Fume hood
- Oven capable of temperatures between 40 °C and 60 °C
- Sample processing microwave *(BioWave, Ted Pella) (optional)*
- Sample processing robot *(ASP1000, Microscopy Innovations) (optional)*
- Ultramicrotome
  - Leica UC6 or UC7 was used for these samples
- Diamond trim tool *(Trim 90, Diatome)*
  - Glass knives and/or razor blades have also been used
- Stereo microscope
- Light microscope
- SEM equipped with a serial block face system
  - *Zeiss Merlin with 3View 2XP was used for these samples*

3.2 Reagents

- Ultrapure Water
- Montjuic Water (See recipe below in protocol)
- 50% aqueous Glutaraldehyde *(Electron Microscopy Sciences #16320)*
- 16% paraformaldehyde solution, EM Grade *(Electron Microscopy Sciences #15710)*
- Sodium cacodylate trihydrate *(Electron Microscopy Sciences #12300)*
- Osmium tetroxide 4% aqueous solution *(Electron Microscopy Sciences #19150)*
- Calcium chloride *(Electron Microscopy Sciences #12340)*
- Sucrose *(Electron Microscopy Sciences #21600)*
- Potassium ferricyanide
- Thiocarbohydrazide *(Electron Microscopy Sciences #21900)*

- Uranyl acetate *(Electron Microscopy Sciences #22400)*
- Lead nitrate *(Electron Microscopy Sciences #17900)*
- Aspartic acid
- Sodium hydroxide pellets
- Acetone-glass distilled *(Electron Microscopy Sciences #10015)*
- Hard Plus resin-812 *(Electron Microscopy Sciences #14115)*
  - Or hard Spurr's formulation (Electron Microscopy Sciences **#14300**)
- Silver conductive epoxy *(Ted Pella, inc. #16043)*
- Pelco colloidal silver liquid *(Ted Pella, inc. #16034)*

3.3 Protocol

3.3.1 Principle

In developing this protocol, we focused on the identification of dividing cells in the largest volume possible. As a starting point, we referenced stage 7 embryo data previously acquired for another application and prepared with a published protocol (Deerinck, Bushong, Ellisman, & Thor, 2022). While the embryo data had good contrast with beautiful dividing cells (Fig. 2A top and bottom) this success did not translate equally to clonally asexual adults, where our imaging attempts lacked in contrast and were full of charging artifacts (data not shown).

To help improve both contrast and conductivity we next tried a protocol designed for difficult-to-penetrate or large samples (Hua, Laserstein, & Helmstaedter, 2015). This protocol gave much better results, but the cell membranes were faint, and tracing them proved to be difficult (Fig. 2B). After consulting a combination of references (Deerinck et al., 2022; Hayat, 2000; Tapia et al., 2012), we decided to modify the first protocol used for the embryo, increasing some staining times to increase conductivity generally and to enhance cell membranes specifically. At the same time, we tested a new resin formulation called Hard Plus, which was said to be as stable for serial block face imaging as those used in the above-referenced protocols and had the benefits of being a relatively low viscosity and easy to acquire (Kizilyaprak, Longo, Daraspe, & Humbel, 2015). While these changes had the intended effect, it left the chromosomes so light they were sometimes nearly impossible to trace for 3D reconstruction (Fig. 2C).

For our third attempt, we decided to combine the longest and most intense staining steps from the previous two protocols, hoping they would combine with their best qualities maintained (Table 2). Using this protocol, we can see DNA/Chromatin staining to identify condensed chromosomes as an identifier for dividing stem cells, as well as largely discern cell membranes to study dividing cell morphology (Fig. 2D). In testing the final protocol, we noted that the heated steps are necessary for the best signal and contrast (Fig. 3). This final protocol is provided below, along with suggested places to change the protocol for the researchers intended outcomes. In our hands, not one protocol fits all cell types.

Table 2 Protocol choices.

Enhanced chromosomes: Hua et al.			Enhanced membranes: Ellison, Tapia, Hyatt			Combined protocol		
Step	**Time**	**Temperature**	**Step**	**Time**	**Temperature**	**Step**	**Time**	**Temperature**
Buffered 2% osmium tetroxide	90 min	Room	Buffered 2% osmium tetroxide 1.5% potassium ferricyanide	Overnight	4 °C	Buffered 2% osmium tetroxide 1.5% potassium ferricyanide	Overnight	4 °C
No Rinse								
Buffered 2.5% potassium ferricyanide	90 min	Room						
Aqueous (TCH)	45 min	40 °C	Aqueous (TCH)	30 min	Room	Aqueous (TCH)	45 min	40 °C
Aqueous 2% osmium tetroxide	90 min	Room	Aqueous 2% osmium tetroxide	2 h	Room	Aqueous 2% osmium tetroxide	2 h	Room
Aqueous 1% uranyl acetate	Overnight	4 °C	Aqueous 1% uranyl acetate	Overnight	Room	Aqueous 1% uranyl acetate	Overnight	4 °C
	2 h	50 °C					2 h	50 °C
Walton's lead aspartate	2 h	50 °C	Walton's lead aspartate	1 h	60 °C	Walton's lead aspartate	2 h	50 °C

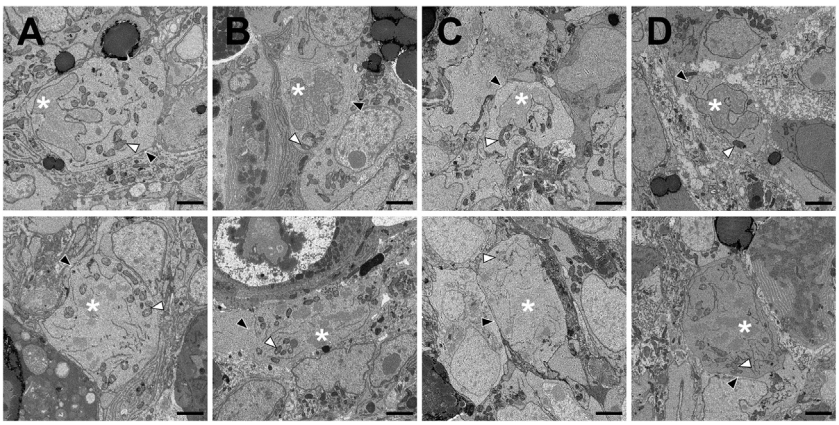

FIG. 2

Comparison of protocols. Representative dividing cells from different protocols. Top row is neoblasts in anaphase where chromosomes are largely encased in nuclear envelope and bottom is prophase (no nuclear envelope). A stage 7 *Smed* embryo (A top and bottom). Asexual adult tissue optimized for chromatin and general organelle staining but poor in cell membrane contrast (B), asexual adult tissue optimized for membranes but poor in chromatin contrast (C), and the merged protocol described here (D). Scale bars are 2 μm. Asterisks = chromosomes, cell membranes = black arrowheads, mitochondria = white arrowheads.

We developed this protocol to run both manually on the bench and with an automated sample processing robot (ASP1000, Microscopy Innovations). The sample processing robot has the advantage of being almost completely hands-off once set up, as well as far faster, given that the robot has continuous rapid agitation and runs after working hours. However, since most labs will not have a robot, we have detailed the manual bench protocol below. This protocol could also most likely be adapted to the use of a sample processing microwave, but the authors have not directly tested that yet.

3.3.2 Sample preparation

Before starting the protocol, please consider the following:

- The protocol assumes that the following have been prepared in advance: fixative and buffer, aqueous osmium (if not purchased), 30 mM L-aspartic acid solution, uranyl acetate, dilutions of acetone to put at 4 °C, and resin

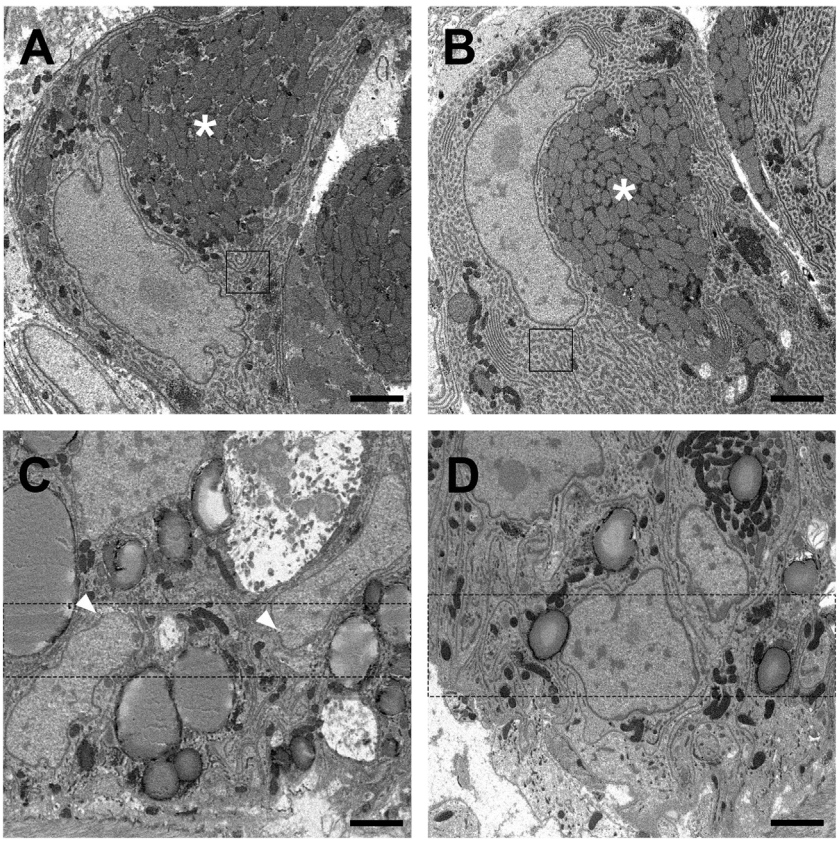

FIG. 3

Comparison of heated vs non-heated steps. Representative secretory cells from a protocol with unheated (A, C) and heated (B, D) steps. Note the poor quality of the secretory granules (asterisk) and noise in (A), making the endoplasmic reticulum (square) less distinct from the surrounding cytoplasm compared to (B) a secretory cell with heated steps. (C) Additionally, unheated steps result in chatter (arrow) at the overlap between montaged XY tiles (dotted box) during acquisition, compared to (D) showing no chatter at acquisition overlaps in samples with heated steps. Working conditions for (A, C): 2.5 kV 300pA, 1.6us dwell, 40% nitrogen. For (B, D) 3 kV, 300pA, 3.2us dwell, 30% nitrogen. Scale bar = 2 μm.

- The timing for all steps is for intact adult *Smed* animals and can be varied depending on sample size, age, and whether the animal is cut into pieces before processing. We have used 2–3 mm animals and strongly suggest cutting animals larger than 3 mm
- A streamlined protocol guide is included (Table 3) which can be reproduced, adapted, and reused as a quick reference sample processing sheet

- Notes and considerations for steps are bullet pointed in italics below each step
- *Chemicals used in sample preparation are toxic*. Please review MSDS sheets before use. All sample preparation steps should be done in a hood with proper protective equipment. Consult with institutional safety protocols for proper disposal procedures
- *All incubations are performed with agitation on a rotator or rocker, except those carried out at higher temperatures inside an oven*

(1) For primary fixation, place intact or fragments of planarian adults/embryos in a small petri dish on top of a cold plate. Wash 3× with Montjuic water (1.6 mmol/L NaCl, 1.0 mmol/L $CaCl_2$, 1.0 mmol/L $MgSO_4$, 0.1 mmol/L $MgCl_2$, 0.1 mmol/L KCl and 1.2 mmol/L $NaHCO_3$ in Milli-Q water, pH 6.9–8.1) (Cebrià & Newmark, 2005). Under a hood, replace the last water rinse with 50 mM sodium cacodylate fixative (2.5% glutaraldehyde 2% paraformaldehyde with 1% sucrose and 1 mM $CaCl_2$ in 50 mM sodium cacodylate) and gently swirl the petri dish a few times. Transfer the specimens to a microcentrifuge or falcon tube with fresh primary fixative within 5 min, where the volume of the fixative is >10× the volume of the sample. Transfer the tubes to a nutator or rocker at 4 °C overnight. Store at 4 °C for at least 24 h and up to 2 weeks before continuing the protocol
- Cold fixation somewhat reduced curling, however we still fixed ~3× the animals needed to obtain enough that were not curled to an unusable extent
- The use of cold will depolymerize microtubules and should not be used if you want to visualize microtubule-based structures
- After primary fixative, for large specimens where only a portion of the animal is of interest, we suggest cutting samples into smaller sizes for the remainder of the protocol
- For marine flatworms, the buffer molarity and perhaps other additive concentrations should be changed to resemble the flatworm's environment more closely. For example, 150–200 mM might be a better buffer molarity for marine species

(2) Remove samples from 4 °C storage and rinse 4 times for 15 min each in 50 mM sodium cacodylate buffer with 1% sucrose and 1 mM $CaCl_2$
- It's important to rinse out all the fixing agents before proceeding to the next steps
- Prepare a 2% reduced osmium solution in 50 mM sodium cacodylate with 1 mM $CaCl_2$ by adding 3% potassium ferricyanide to 100 mM sodium cacodylate buffer with 2 mM CaCl2 and mixing 1:1 with 4% aqueous osmium tetroxide, for use in Step 3

(3) Incubate the samples in the 2% reduced osmium solution prepared above for 4 h at room temperature or overnight at 4 °C
- Osmium tetroxide post-fixation helps stabilize lipids as well as adds contrast and conductivity to the sample

- During this step prepare the thiocarbohydrazide (TCH) solution for step 5 by dissolving 0.1 g TCH in 10 mL of ultrapure water by either placing it in a 60 °C oven and swirling every 10 min, or on a hot plate with a stir bar

(4) Rinse samples 4 times for 15 min each in ultrapure water
- At this step it is important to rinse out any reduced osmium not bound to the sample to prepare for the TCH

(5) Incubate the samples in freshly filtered TCH solution at 40 °C–60 °C for 45 min
- TCH binds to osmium and will bind additional osmium in Step 7 below, amplifying heavy metal staining and increasing contrast and the conductivity of the sample as well as conferring structural stability (Forge, Nevill, Zajic, & Wright, 1992)
- We have used 40 °C, 50 °C, and 60 °C for this step

(6) Rinse samples 4 times for 15 min each in ultrapure water

(7) Incubate the samples in 2% aqueous osmium tetroxide for 2 h at room temperature

(8) Rinse samples 4 times for 15 min each in ultrapure water

(9) Incubate the samples in 1% aqueous uranyl acetate (UA) overnight at 4 °C
- UA is a common En Bloc stain in electron microscopy which aids in preservation and adds contrast and conductivity to the sample

(10) The next morning, transfer the samples, still in 1% UA, to 50 °C–60 °C for 2 h
- The long portion of this incubation allows time for the slow-moving UA to penetrate throughout the tissue, while the heated step enhances the binding of UA to proteins and membranes (Hua et al., 2015)
- We have used 50 °C and 60 °C for this step

(11) Rinse samples 4 times for 15 min each in ultrapure water
- At this step it is important to rinse out any UA not bound to the sample to prepare for the lead staining
- During this step, prepare lead aspartate solution for use in Step 12 by dissolving 0.066 g lead nitrate in 10 mL of 30 mM L-aspartic acid. Add sodium hydroxide to pH of 5.5. The solution should be clear when ready for use

(12) Incubate the samples in lead aspartate at 50 °C–60 °C for 2 h
- This will further enhance the contrast and conductivity of the sample.
- We have used 50 °C and 60 °C for this step

(13) Rinse samples 4 times for 15 min each in ultrapure water
- At this step it is important to rinse out any heavy metals not bound to the sample to prevent precipitate contamination during dehydration

(14) Incubate samples in pre-cooled 25%, 50%, 75%, 90% and 100% pre-cooled acetone for 15 min each on ice

- We used acetone in 25%, 50%, 75%, and 90%, dilutions, but dehydration schedules vary greatly, and some prefer ethanol and/or use a transitional solvent like propylene oxide
- We have done this step at 4 °C and room temperature did not notice any appreciable difference

(15) Exchange the 100% acetone for fresh pre-cooled 100% acetone and move the samples to room temperature for 15 min

(16) Incubate one more time with 100% acetone for 15 min at room temperature

- During this step prepare 25% Hard Plus resin in acetone. Make sure both resin and acetone are at room temperature and mix well until no swirls are seen

(17) Incubate samples in 25% resin for 30 min to 1 h

- When done manually on the bench, this protocol takes a 9-h day, so we usually make sure the 25% dilution goes for at least 30 min before exchanging to the next dilution for overnight incubation
- Save time by preparing each dilution during the last 10 min or so of the previous step
- With the ASP-1000 sample processing robot, resin steps up to 75% were set to 30 min each at a pump speed between 8 (72 exchanges per minute) and 12 (55 exchanges per minute)

(18) Incubate in 50% resin in acetone overnight at room temperature

(19) In the morning, prepare 75% resin in acetone and incubate samples at room temperature

- For hard-to-infiltrate samples: At 75% and 100% infiltration steps we used a sample processing microwave (BioWave, Ted Pella) at 250 W for 3 min on, 3 min off, and 3 min on, on a cold spot under vacuum. We put only 0.5 mL in each tube while in the microwave and topped it off to a final volume of 1.5 mL before placing it on the sample rotator

(20) In the afternoon and again at the end of the day, incubate the samples in 100% resin with a microwave (if available) and place them on a rotator in between incubations and overnight

- Because the resin is very viscous at 100%, we use a vertical sample rotator for these steps
- With the ASP-1000 sample processing robot, 100% resin steps were set to 2 h each at a pump speed of 21 (8 exchanges per minute) for 2 exchanges, and a third resin exchange left overnight with no exchanges per minute

(21) In the morning perform one final 100% resin incubation as above

Table 3 Quick reuse sample processing sheet.

Planarian SBF-SEM

*Make: 0.1M sodium cacodylate with 2mM CaCl2, aspartic acid stock, Hard Plus resin

Primary Fixation 4C:

Buffer Rinses- 0.05M sodium cacodylate buffer (1mM CaCl2 and 1% sucrose) 4X15m

2% Aqueous OsO4 in 50mM sodium cacodylate with 1mM CaCl2
Add 3% potassium ferricyanide to 0.1M sodium cacodylate with 2mM CaCl2 and mix 1:1 with 4% aqueous OsO4
4 hours RT or ON at 4C:
ULTRAPURE WATER RINSES: 4x15min EACH room temp

*make TCH: 0.1g TCH 10ml ddH2O, swirl every 10 minutes in 60C oven for 1h or on hot plate with stir bar @60C

TCH Solution: 0.22um filtered
45 min @45C- 60C:
ULTRAPURE WATER RINSES:4x15min EACH room temp

2% Aqueous OsO4
2 Hours RT:
ULTRAPURE WATER RINSES: 4x15min EACH room temp

1% Aqueous uranyl acetate
Overnight at 4C:

1% Aqueous uranyl acetate
Move to 50C- 60C 2 hours:
ULTRAPURE WATER RINSES: 4x15min EACH.

*make lead aspartate: 0.066g Pb nitrate in 10ml aspartic acid adjust pH to 5.5

Walton's Pb Solution
50- 60C 2 hours:
ULTRAPURE WATER RINSES: 4x15min EACH room temp

DEHYDRATION
ACETONE: **15min on ice**
25% 50% 75% 90% 100%
100%

RESIN INFILTRATION: Hard Plus Resin
25% Hard Plus: 75% Hard Plus: 100% Hard Plus:
50% Hard Plus: 100% Hard Plus:
75% Hard Plus: 100% Hard Plus:

SAMPLE EMBEDDED AND POLYMERIZED 60C for 48 hours

3.3.3 Sample embedding

Samples were embedded in flat molds or Beem capsules, minimally resin embedded (Schieber et al., 2017) or embedded directly on 3View pins (Gatan) using conductive silver epoxy. Samples were flat embedded either with the desired imaging area closest to the cutting plane of the block or furthest from the cutting plane of the block, depending on intended pin mounting strategies described below. Samples embedded directly on pins had extra resin removed from the unpolymerized sample before placing on the pin with conductive epoxy (not shown). Once placed in molds or on pins, all samples were polymerized at 60 °C in an oven for 48 h or over a weekend. To avoid brittleness in the polymerized samples, we have embedded in filled Beem capsules with the lid on.

3.3.4 Preparation for SBF-SEM

Samples embedded in flat molds or Beem capsules were loaded into a microtome and either faced into until almost reaching the desired imaging area (prescreen) or until tissue was reached (post screen), depending on the chosen embedding orientation. The samples were then carefully cut from the larger resin block. When necessary, the samples were carefully trimmed under a dissecting microscope using a razor blade, either to reduce the overall size or to expose tissue for direct contact with the pin in the case of a prescreen embedding strategy. Conductive epoxy was prepared according to the instructions, and a small amount placed onto a pin. The sample was pushed into the epoxy with the area of interest facing away from the pin in the desired orientation for cutting, so that the sample is in contact with the pin surface and surrounded and supported by the conductive epoxy (Fig. 4).

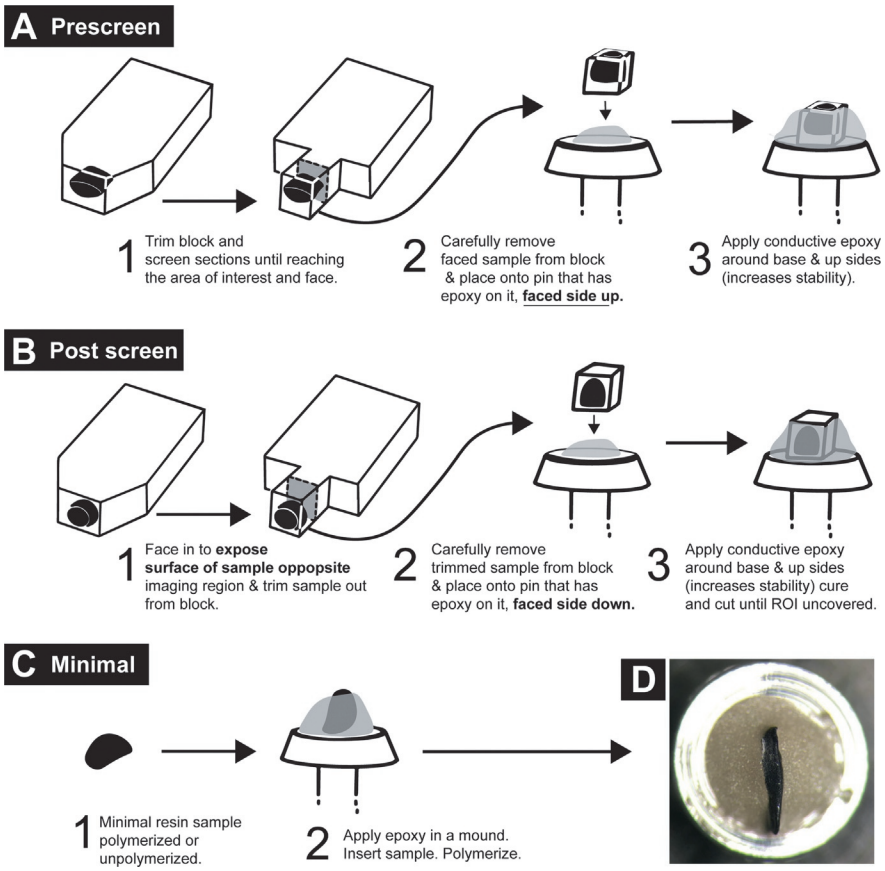

FIG. 4

Schematics of mounting samples onto the pin for 3View. (A) Prescreen, (B) Post screen and (C) Minimal methods for mounting samples onto pins. (D) Top down view of sample for final result of the Minimal approach, note there is no block shape or empty resin.

Polymerized samples mounted on pins were placed back into a 60 °C oven overnight to cure the conductive epoxy.

After curing, the samples on pins were faced to the area of interest with an ultramicrotome, and the samples were assessed for quality if not prescreened before mounting. Quality assessment for all samples was done either by cutting and viewing sections in a TEM or SEM, or loading the block into the SEM to directly image the block-face. If necessary, the sample block-face was trimmed down to a square or rectangle <1 mm in X and Y at 150 μm depth (Fig. 5). Finally, prepared and faced pins were painted with silver paint or coated with metal in a sputter coater to aid conductivity before loading into the 3View system.

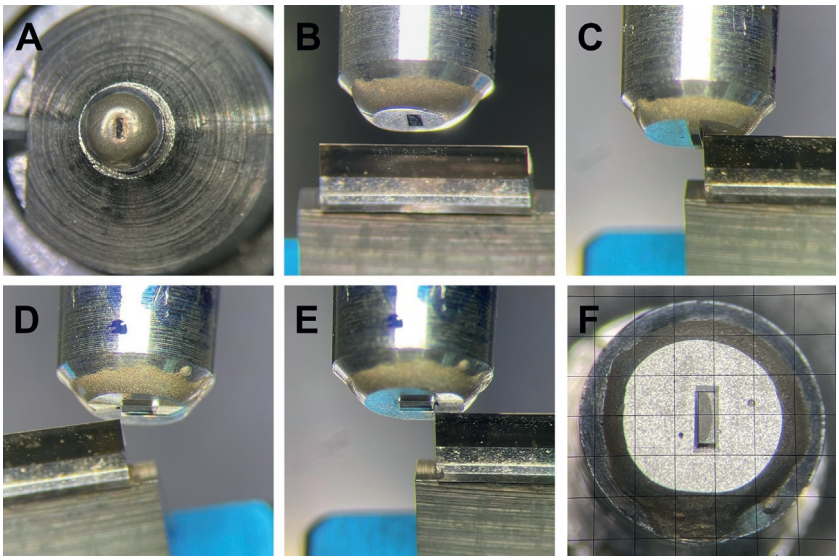

FIG. 5

Stepwise preparation of the 3View Pin block-face. (A) View of a sample mounted on a pin with conductive epoxy in the sample holder designed for use with an ultramicrotome. (B) The sample is sectioned with a glass or diamond knife, exposing the area of interest to be imaged. The block-face is then (C–E) trimmed to remove the resin on all sides of the sample with a 90-degree trim tool to 150 μm in depth, and such that the specimen is (F) <1 mm in X and Y. Grid in (F) is 0.5 mm.

3.3.5 Imaging

The prepared sample pin was loaded into the 3View system for the approach as detailed in the manual. Briefly, the pin was centered in the holder with the area needed for acquisition positioned closest to the center and opposite the screw on

the holder. This ensured the area of interest was closest to the nitrogen gas delivery tube of the focal charge system (Zeiss) (Deerinck et al., 2018). The holder was then loaded into the system, the stage zeroed, and the knife adjusted so the cutting window will cover the whole block face during the cutting stroke. Making sure the knife is in the stroke-up position, the surface of the block was then manually raised toward the knife, as close as possible without contact, and the software was set to cut sections of between 100 and 200 nm thickness until the whole block face was being cut by the knife. At this point, if your system is equipped with focal charge compensation, the nitrogen gas delivery tube can be centered and placed appropriately close to the area to be imaged, generally around 200 μm away (Fig. 6). During cutting, the tube is pushed forward out of the way and will swing back to the placed position to deliver nitrogen gas to the block-face only during imaging. It is important to take distance from the focal charge compensator into account, as the effect varies over distance (Fig. 7). Images acquired too close to the nitrogen source will be unnecessarily decreased in contrast, while areas too far away will not have adequate charge compensation even at 100% nitrogen. Once the focal charge compensator set up is complete, the knife is cleared of sections and the chamber is closed for the system to be pumped down.

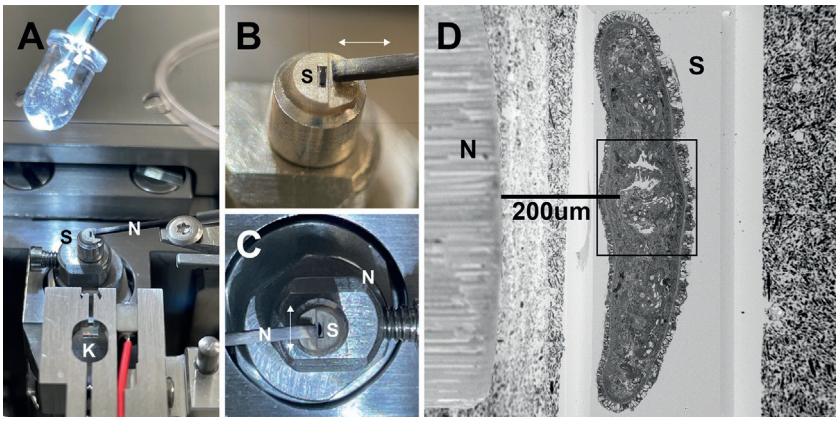

FIG. 6

Correct positioning of Focal Charge Compensator. (A) Overview of a sample loaded into the 3View system. (B) Nozzle placement positioned close to the sample as viewed from the side, double arrow indicates direction of adjustment. (C) Nozzle placement centered on the sample as viewed from above, double arrow indicates direction of adjustment. (D) SEM image showing nozzle placement centered as accurately as possible on the area of interest and placed approximately 200 μm away from the middle of the region of interest. S = Sample, N = focal charge compensator nitrogen nozzle, K = knife.

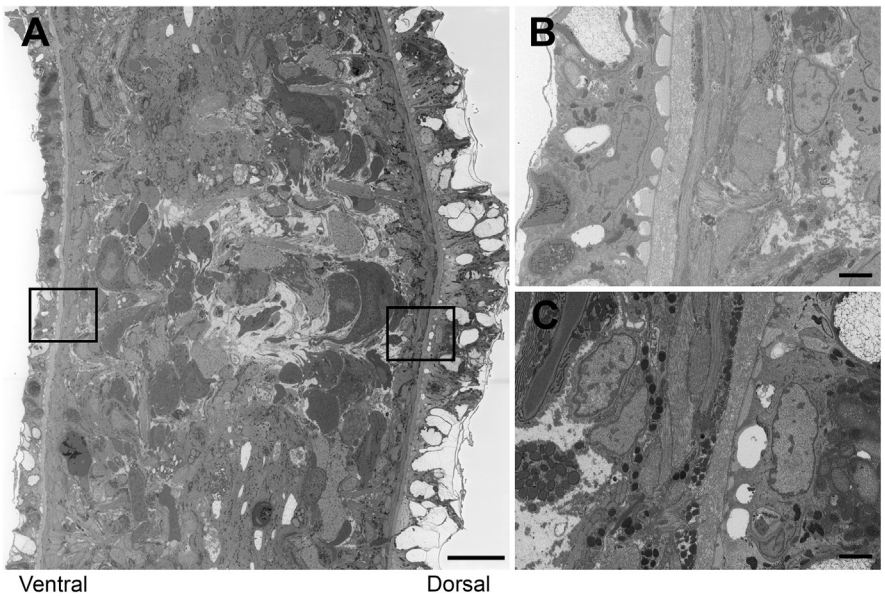

FIG. 7

Effects of the Focal Charge Compensator. (A) Overview of Smed showing effects of the focal charge compensator, where in 202 μm wide field of view, the area closest to the nitrogen source (B) will be reduced in contrast compared to regions further from the focal charge compensator (C). This gradient requires consideration for a single field of view as well as XY montage tile histogram normalization for downstream analysis. Scale bars are 20 μm in panel (A) and 2 μm in panels (B, C).

We used both Gatan Microscopy Suite and SBEMimage acquisition software (Titze, Genoud, & Friedrich, 2018). Working conditions for the adult asexual Smed were 3 kV and 300pA with nitrogen levels for FCC set to 30–40% and pixel dwell time at 3.2us. Pixel size in XY was 15 nm and slice thickness was 60 nm. Montages with tile size up to 10,000 pixels^2 and total imaging areas up to 182 μm in X, 420 μm in Y with Z slice numbers up to 1700 were acquired (data not shown). The maximum area imaged without significant distortion at the edges varied between 68 μm at 10,000 pixels for 1.1 kV (6.9 mm working distance) and 150 μm at 10,000 pixels for 3 kV (6.1 mm working distance).

3.4 Analysis

3.4.1 Alignment

Resulting data was stitched in XY using grid stitching in Image J (Preibisch, Saalfeld, & Tomancak, 2009). XY montage tiles were histogram normalized. Z alignment was carried out using IMOD (Kremer, Mastronarde, & McIntosh, 1996). We also normalized the XY histograms across the Z direction using a python script (AlignTools/correct_z_intensity.ipynb at master · cwood1967/AlignTools · GitHub) based on previously published work (Vergara et al., 2021), which greatly improved the downstream deep learning workflows.

3.4.2 Segmentation

3.4.2.1 Manual

Segmentation of complex and variable structures was carried out by hand using the drawing tools function in IMOD (Kremer et al., 1996). Highly variable and unpredictable shapes or structures were traced in every section; for large uniform structures like outlining tissues (i.e., gut), we traced at intervals of 5–10 slices. Once the structure was traced and meshed, meshes were exported as wavefront files for subsequent visualization.

3.4.2.2 Deep learning

Well-stained, highly contrasted and plentiful structures (i.e., nuclei) were segmented using deep learning via DeepFiji (Fig. 8). DeepFiji is a Deep Learning platform comprised of a collection of plugins and macros in Fiji, Python, and CherryPy (python web framework) (Nuckolls et al., 2020). We have also had some good experiences using Ilastik pixel classification for 3D deep learning on structures (not shown). Segmentation (or probability files) from deep learning workflows were run through Fiji's 3D Viewer (Schmid, Schindelin, Cardona, Longair, & Heisenberg, 2010) as surfaces and exported as wavefront files for subsequent visualization.

3.4.3 Visualization

To visualize whole 3D volumes without segmentation, we prefer Amira with heavily binned data (bin of ~20 for 15 nm pixel XY resolution of original), as it loads and visualizes quickly (Fig. 9). To best visualize both deep learning and manual

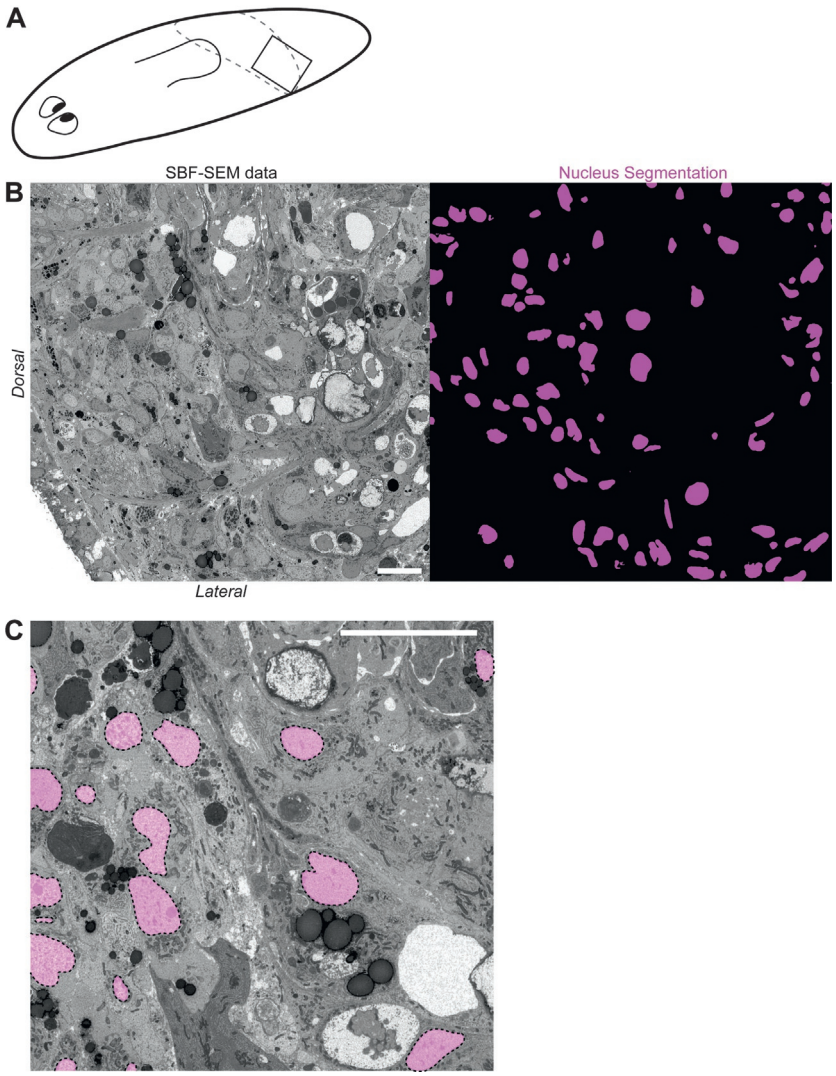

FIG. 8

Deep Learning Segmentation of Nuclei. (A) Data showing the post-pharyngeal, lateral, and dorsal edge of a planarian that was (B) segmented for nuclei using DeepFiji. (C) Close-up of nuclear segmentation overlaid on the SBF-SEM data in magenta/white and outlined with black dashes. Scale bars = 20 μm.

segmentations from the data, we render the imported wavefront files in Blender (Community, 2018) (Figs. 10 and 11, Movies 1 and 2 in the online version at https://doi.org/10.1016/bs.mcb.2023.01.013). While there are multiple software options for 3D rendering, we use Blender because it is open source, python compatible, there are plentiful videos and tutorials on its use, as well as an active Stack Overflow community to help with questions.

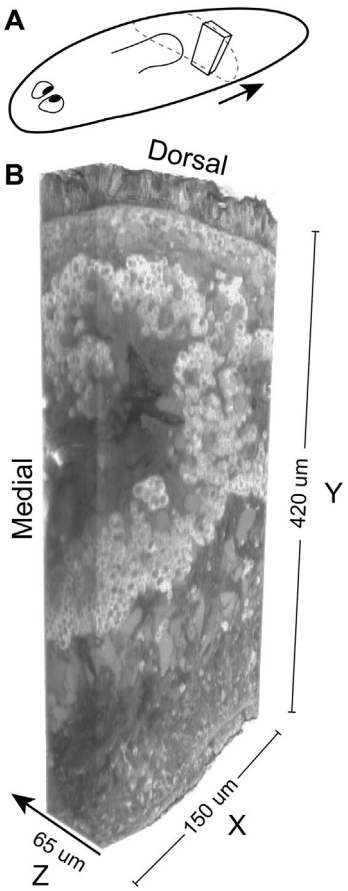

FIG. 9

Rendering data volumes with Amira. (A) Location in *Smed* of an example volume with the direction of cutting indicated by arrow.(B) Amira rendered volume of a mediolateral post pharyngeal region encompassing 65 μm deep (anterior-posterior axis), 150 μm wide (mediolateral axis), and 420 μm tall (dorsoventral axis). XYZ indicates imaging orientation with arrow showing direction of cutting.

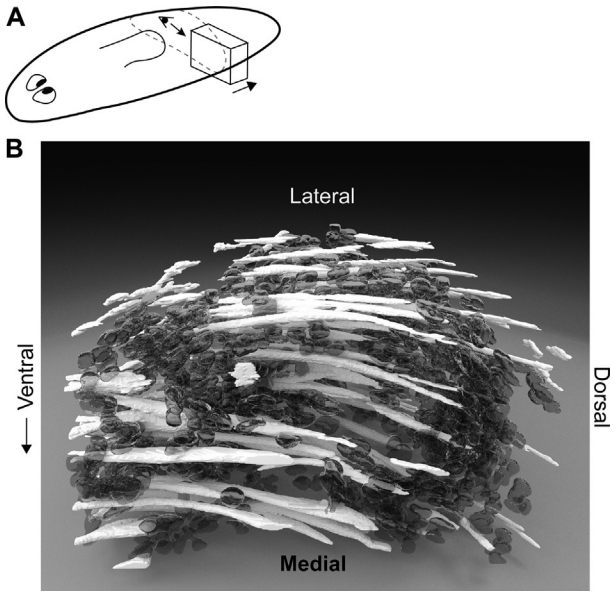

FIG. 10

Rendering segmented data with Blender. Blender rendering of a data volume 150 μm in XY (dorsoventral and mediolateral) and 90 μm (anterior-posterior) taken from (A) post pharyngeal region encompassing medial to the lateral edge that was (B) segmented for nuclei (gray glassy texture) and muscle fibers (white rods). Viewpoint for render is from medial in foreground to lateral edge in background with dorsal to the right and ventral to the left. Arrows in both panels indicate direction of cutting.

4 Summary

4.1 A note on safety

As with all laboratory experiments, for your safety following this protocol please familiarize yourself with the MSDS datasheets of all chemicals involved. MSDS sheets can generally be found within your lab, university or institution, or vendor's website. All the sample preparation should be done in a hood with ventilation and the appropriate personal protective equipment, including but not limited to lab coat, nitrile gloves, and protective eye wear. Protect fingers and eyes during the block mounting steps when using a razor blade to remove plastic resin pieces by going slow and wearing protective eye wear.

4.2 Discussion

There are limitations to all experiments, especially microscopy experiments where many antagonistic factors must be brought to a favorable balance to achieve the desired outcome. In SBF-SEM work there are concrete physical limits at the time

of acquiring the data as well as more nebulous limits in time and knowledge before and after data acquisition. The clear physical limiting factors in SBF-SEM to take into consideration are field-of-view, resolution, and destruction. The current field of view limitations are most strongly influenced by both the stage travel and the knife cutting window limits. The resolution sits in the 10–50 nm^3 region (Peddie et al., 2022), and the method is destructive. In our exploration of SBF-SEM for planarian worms, image resolution and clarity were balanced with time and volume size. If speed is prioritized by using a faster pixel dwell time, a greater total volume of data can be acquired faster but the signal to noise ratio will be altered and finer details may be lost to noise. Even with an optimized protocol, acquisition parameters such as section thickness and pixel dwell time impact the clarity and resolution of these features and consequently the ability to reliably follow features through a volume.

For increased resolution beyond what SBF-SEM can provide, moving to a FIB-SEM approach will have the same automated benefits of SBF-SEM with higher voxel resolution, but acquisition time will limit the total volume which can be acquired in a defined amount of time. If your area of interest is very small, serial section TEM tomography is an option. If you require a larger volume and need to have archival samples for reimaging later, consider moving to a microtome based automated serial section on tape approach such as the ATUMtome (RMC Boeckeler) for SEM array tomography or the Blade (Voxa) for use with a modified TEM. If your volume needs are smaller but you still require archival sections, consider array tomography of serial sections mounted on slides or coverslips. In general, volume electron microscopy approaches using an SEM will have a greater flexibility in section size and therefore maximum field of view than TEM approaches.

Key time and knowledge limiting steps in SBF-SEM include sample preparation protocol troubleshooting, area of interest targeting, and post-processing data extraction. While developing sample preparation protocols for planarian worms, we explored many avenues in hopes of gaining an advantage in either quality, area of interest targeting, or just general time savings. The protocol presented here represents key parameters in our success, but we also observed some subtle differences in outcomes between sample runs which could guide further streamlining and adaptation. Differences in stain intensity and membrane contrast were the most obvious. While more experimentation with these parameters is necessary to narrow down the exact cause, in our experience samples run with staining temperatures of 60 °C had better signal to noise, while temperatures at 50 °C had more cell membrane contrast. Another contributing factor for this outcome could be total time spent in resin dilution steps. In our explorations with general time saving by using the ASP1000 robot, we were able to set all resin dilution steps to 30 min and proceed directly to pure resin incubations, eliminating the overnight incubation in 50% resin and shortening the incubation in 75% resin. Since we have not run samples with 60 °C staining steps combined with shorter resin dilution times, it remains to be seen if time spent in resin dilutions has an effect. Differences were not apparent between samples with the same resin dilution time but longer time spent in 100% resin. Nor were differences apparent between samples run with overnight staining steps at 4 °C compared to 4 h at

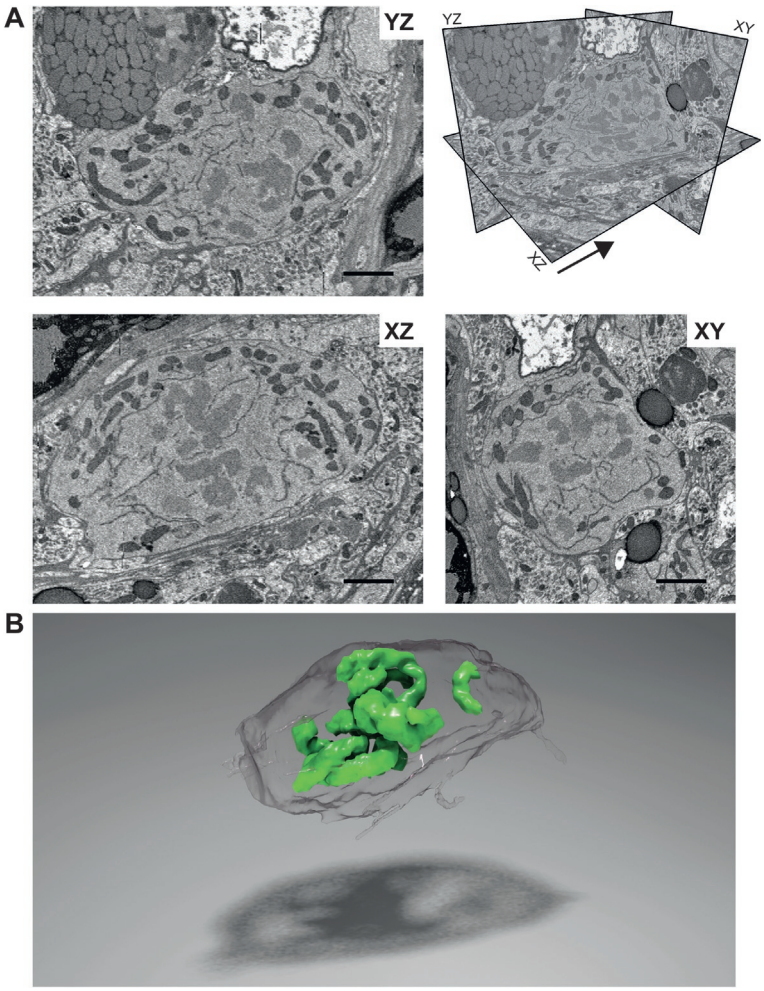

FIG. 11

Rendering of manually segmented prophase mitotic cell with Blender. (A) Orthogonal views of the data containing a prophase neoblast in an adult asexual *Smed* with direction of cutting and XY acquisition noted with an arrow (B) rendered in Blender with the cell membrane in clear and the chromosomes in green.

room temperature. Using the sample processing robot, we were able to significantly shorten the protocol compared to manual bench processing and still achieve good results for our intended purpose (Fig. 11).

For area of interest targeting, all of our embedding and mounting strategies had a mixture of advantages and drawbacks that made it difficult to give a general

recommendation. For example, minimal resin and direct pin mounting were time savers and allowed for the area of interest to be targeted quite easily, but came with pitfalls of brittleness and samples that were difficult to mount straight without being obscured by the conductive resin. Once the sample is covered with opaque conductive resin, achieving correct orientation can be very difficult. If the sample was embedded using the prescreening strategy (Fig. 5A), an advantage is that the best samples can be chosen by screening at or near the area of interest before the extra step of mounting on pins. This comes with the disadvantage that it will be more difficult to mount the sample flat on the pin with the desired orientation, since preparation of the side which goes against the pin will have to be trimmed flat by hand with a razor blade once the sample is removed from the block. The post screening strategy made it very easy to orient the samples on the pin so that the area of interest was parallel to the flat surface created by cutting into the tissue. The heavy metal stained tissue is placed directly against the metal pin with the conductive epoxy, aiding in conductivity (Fig. 5B). However, the drawback of mounting samples on pins before finding and checking the actual area of interest meant we tended to default back to screening samples still in blocks before mounting, even though that made mounting on the pin at the right orientation more difficult.

Here, we offer this protocol as a springboard for exploring the cellular details of aquatic invertebrates and fellow phylum members. Specifically, interrogation of *Smed* relatives that are currently capable of transgenesis (Wudarski et al., 2017) and those that may have a different cellular-level regenerative response (Duncan et al., 2022) will be of interest. With respect to downstream post-processing data extraction, we are greatly looking forward to deep learning, AI-mediated segmentation and data extraction becoming more accessible, allowing smaller teams access to faster big data exploration.

Acknowledgments

A big thanks to Erin Davies for the embryos for early work; Morgan Greenwood for robot protocol optimization; Xia Zhao for help with bench sample processing; Mol Mir for work on tracing, training, rendering, and illustrations; Chris Wood for work on alignment workflows; Sean McKinney for DeepFiji; and Alejandro Sánchez Alvarado for continual optimism, support, and patience through a *lot* of optimizing. Original data underlying this manuscript can be accessed from the Stowers Original Data Repository at http://www.stowers.org/research/publications/libpb-1728.

References

Auladell, C., Garcia-Valero, J., & Baguñà, J. (1993). Ultrastructural localization of RNA in the chromatoid bodies of undifferentiated cells (neoblasts) in planarians by the RNase-gold complex technique. *Journal of Morphology*, *216*(3), 319–326.

Baguñà, J. (1976). Mitosis in the intact and regenerating planarian Dugesia mediterranea n.sp. II. Mitotic studies during regeneration, and a possible mechanism of blastema formation. *The Journal of Experimental Zoology*, *195*(1), 65–79.

Baguñà, J., Saló, E., & Auladell, C. (1989). Regeneration and pattern formation in planarians. III. Evidence that neoblasts are totipotent stem cells and the source of blastema cells. *Development*, *107*, 77–86.

Cebrià, F., & Newmark, P. A. (2005). Planarian homologs of netrin and netrin receptor are required for proper regeneration of the central nervous system and the maintenance of nervous system architecture. *Development*, *132*(16), 3691–3703.

Community, B. O. (2018). *Blender - a 3D modelling and rendering package*. Blender Foundation. http://www.blender.org.

Coward, S. J. (1968). The relation of surface and volume to so-called physiological gradients in planaria. *Developmental Biology*, *18*(6), 590–601.

Deerinck, T. J., Bushong, E. A., Ellisman, M. H., & Thor, A. (2022). *Preparation of biological tissues for serial block face scanning Electron microscopy (SBEM)*. Protocols.Io.

Deerinck, T. J., Shone, T. M., Bushong, E. A., Ramachandra, R., Peltier, S. T., & Ellisman, M. H. (2018). High-performance serial block-face SEM of nonconductive biological samples enabled by focal gas injection-based charge compensation. *Journal of Microscopy*, *270*(2), 142–149.

Duncan, E. M., Nowotarski, S. H., Guerrero-Hernández, C., Ross, E. J., D'Orazio, J. A., Clubes de Ciencia México Workshop for Developmental Biology, et al. (2022). Molecular characterization of a flatworm Girardia isolate from Guanajuato, Mexico. *Developmental Biology*, *489*, 165–177.

Forge, A., Nevill, G., Zajic, G., & Wright, A. (1992). Scanning electron microscopy of the mammalian organ of Corti: Assessment of preparative procedures. *Scanning Microscopy*, *6*(2), 521–534. discussion 534–535.

Grudniewska, M., Mouton, S., Grelling, M., Wolters, A. H. G., Kuipers, J., Giepmans, B. N. G., et al. (2018). A novel flatworm-specific gene implicated in reproduction in Macrostomum lignano. *Scientific Reports*, *8*(1), 3192.

Hay, E. D., & Coward, S. J. (1975). Fine structure studies on the planarian, Dugesia. I. Nature of the "neoblast" and other cell types in noninjured worms. *Journal of Ultrastructure Research*, *50*(1), 1–21.

Hayat, M. A. (2000). *Principles and techniques of Electron microscopy biological applications* (4th Edition). Cambridge University Press.

Hori, I. (1982). An ultrastructural study of the chromatoid body in planarian regenerative cells. *Journal of Electron Microscopy*, *31*, 63–72.

Hori, I. (1992). Localization of laminin in the subepidermal basal lamina of the planarian Dugesia japonica. *The Biological Bulletin*, *183*(1), 78–83.

Hua, Y., Laserstein, P., & Helmstaedter, M. (2015). Large-volume en-bloc staining for electron microscopy-based connectomics. *Nature Communications*, *6*, 7923.

Kim, I. V., Duncan, E. M., Ross, E. J., Gorbovytska, V., Nowotarski, S. H., Elliott, S. A., et al. (2019). Planarians recruit piRNAs for mRNA turnover in adult stem cells. *Genes & Development*, *33*(21−22), 1575–1590.

Kizilyaprak, C., Longo, G., Daraspe, J., & Humbel, B. M. (2015). Investigation of resins suitable for the preparation of biological sample for 3-D electron microscopy. *Journal of Structural Biology*, *189*(2), 135–146.

Kremer, J. R., Mastronarde, D. N., & McIntosh, J. R. (1996). Computer visualization of three-dimensional image data using IMOD. *Journal of Structural Biology*, *116*(1), 71–76.

Montgomery, J., & Coward, S. (1974). On the minimal size of a planarian capable of regeneration. *Transactions of the American Microscopical Society*, *93*(3), 386–391.

Morgan, T. (1898). Experimental studies of the regeneration of Planaria maculata. *Wilhelm Roux' Archiv Fur Entwicklungsmechanik Der Organismen*, *7*, 364–397.

Morita, M. (1967). Observation on the fine structure of the neoblast and its cell division in the regenerating planaria. *Science reports of Tohoku University Fourth Series. Biology*, *33*, 399–406.

Morita, M., Best, J. B., & Noel, J. (1969). Electron microscopic studies of planarian regeneration. I. Fine structure of neoblasts in Dugesia dorotocephala. *Journal of Ultrastructure Research*, *27*(1), 7–23.

Newmark, P. A., & Sánchez Alvarado, A. (2000). Bromodeoxyuridine specifically labels the regenerative stem cells of planarians. *Developmental Biology*, *220*(2), 142–153.

Nuckolls, N. L., Mok, A. C., Lange, J. J., Yi, K., Kandola, T. S., Hunn, A. M., et al. (2020). The wtf4 meiotic driver utilizes controlled protein aggregation to generate selective cell death. *eLife*, *9*. https://doi.org/10.7554/eLife.55694.

Orii, H., Sakurai, T., & Watanabe, K. (2005). Distribution of the stem cells (neoblasts) in the planarian Dugesia japonica. *Development Genes and Evolution*, *215*(3), 143–157.

Oviedo, N. J., Newmark, P. A., & Sánchez Alvarado, A. (2003). Allometric scaling and proportion regulation in the freshwater planarian Schmidtea mediterranea. *Developmental Dynamics: An Official Publication of the American Association of the Anatomists*, *226*(2), 326–333.

Peddie, C. J., Genoud, C., Kreshuk, A., Meechan, K., Micheva, K. D., Narayan, K., et al. (2022). Volume electron microscopy. *Nature Reviews Methods Primers*, *2*(1), 1–23.

Pedersen, K. J. (1959). Cytological studies on the planarian neoblast. *Zeitschrift Fur Zellforschung Und Mikroskopische Anatomie*, *50*, 799–817.

Pellettieri, J., Fitzgerald, P., Watanabe, S., Mancuso, J., Green, D. R., & Sánchez Alvarado, A. (2010). Cell death and tissue remodeling in planarian regeneration. *Developmental Biology*, *338*(1), 76–85.

Preibisch, S., Saalfeld, S., & Tomancak, P. (2009). Globally optimal stitching of tiled 3D microscopic image acquisitions. *Bioinformatics*, *25*(11), 1463–1465.

Reddien, P. W., & Sánchez Alvarado, A. (2004). Fundamentals of planarian regeneration. *Annual Review of Cell and Developmental Biology*, *20*, 725–757.

Rouhana, L., Weiss, J. A., King, R. S., & Newmark, P. A. (2014). PIWI homologs mediate histone H4 mRNA localization to planarian chromatoid bodies. *Development*, *141*(13), 2592–2601.

Salvetti, A., Rossi, L., Deri, P., & Batistoni, R. (2000). An MCM2-related gene is expressed in proliferating cells of intact and regenerating planarians. *Developmental Dynamics: An Official Publication of the American Association of the Anatomists*, *218*(4), 603–614.

Schieber, N. L., Machado, P., Markert, S. M., Stigloher, C., Schwab, Y., & Steyer, A. M. (2017). Minimal resin embedding of multicellular specimens for targeted FIB-SEM imaging. *Methods in Cell Biology*, *140*, 69–83.

Schmid, B., Schindelin, J., Cardona, A., Longair, M., & Heisenberg, M. (2010). A high-level 3D visualization API for Java and ImageJ. *BMC Bioinformatics*, *11*, 274.

Solana, J., Lasko, P., & Romero, R. (2009). Spoltud-1 is a chromatoid body component required for planarian long-term stem cell self-renewal. *Developmental Biology*, *328*(2), 410–421.

Tapia, J. C., Kasthuri, N., Hayworth, K. J., Schalek, R., Lichtman, J. W., Smith, S. J., et al. (2012). High-contrast en bloc staining of neuronal tissue for field emission scanning electron microscopy. *Nature Protocols*, *7*(2), 193–206.

Titze, B., Genoud, C., & Friedrich, R. W. (2018). SBEMimage: Versatile acquisition control software for serial block-face electron microscopy. *Frontiers in Neural Circuits*, *12*, 54.

Vergara, H. M., Pape, C., Meechan, K. I., Zinchenko, V., Genoud, C., Wanner, A. A., et al. (2021). Whole-body integration of gene expression and single-cell morphology. *Cell*. https://doi.org/10.1016/j.cell.2021.07.017.

White, J. G., Southgate, E., Thomson, J. N., & Brenner, S. (1986). The structure of the nervous system of the nematode Caenorhabditis elegans. *Philosophical Transactions of the Royal Society of London. Series B, Biological Sciences*, *314*(1165), 1–340.

Wudarski, J., Simanov, D., Ustyantsev, K., de Mulder, K., Grelling, M., Grudniewska, M., et al. (2017). Efficient transgenesis and annotated genome sequence of the regenerative flatworm model Macrostomum lignano. *Nature Communications*, *8*(1), 1–12.